Title

Characterizing the metabolic profile of dexamethasone treated human trabecular meshwork cells

Authors

Graybeal, Kimberly
Sanchez, Luis
Zhang, Chi
et al.

Publication Date

2022

DOI

10.1016/j.exer.2021.108888

Peer reviewed

HHS Public Access

Author manuscript

Exp Eye Res. Author manuscript; available in PMC 2022 July 11.

Published in final edited form as:

Exp Eye Res. 2022 January ; 214: 108888. doi:10.1016/j.exer.2021.108888.

Characterizing the metabolic profile of Dexamethasone treated human trabecular meshwork cells

Kimberly Graybeal[1], **Luis Sanchez**[1], **Chi Zhang**[1], **Linsey Stiles**[2], **Jie J. Zheng**[1,*]

[1]Stein Eye Institute, Department of Ophthalmology, David Geffen School of Medicine and The Molecular Biology Institute at the University of California, Los Angeles, Los Angeles, CA, USA

[2]Department of Medicine, Endocrinology, and Department of Molecular and Medical Pharmacology, David Geffen School of Medicine, University of California, Los Angeles, CA, USA

Abstract

The trabecular meshwork (TM) is the leading site of aqueous humor outflow in the eye and plays a critical role in maintaining normal intraocular pressure. When the TM fails to maintain normal intraocular pressure, glaucoma may develop. Mitochondrial damage has previously been found in glaucomatous TM cells; however, the precise metabolic activity of glaucomatous TM cells has yet to be quantitatively assessed. Using dexamethasone (Dex) treated primary human TM cells to model glaucomatous TM cells, we measure the respiratory and glycolytic activity of Dex-treated TM cells with an extracellular flux assay. We found that Dex-treated TM cells had quantifiably altered metabolic profiles, including increased spare respiratory capacity and ATP production rate from oxidative phosphorylation. Therefore, we propose that reversing or preventing these metabolic changes may represent an avenue for future research.

Keywords

Trabecular meshwork; primary open angle glaucoma; myocilin; mitochondria

Elevated intraocular pressure (IOP) is a primary risk factor for the development of glaucoma, a leading cause of irreversible blindness that affects over 70 million people across the world, with primary open-angle glaucoma (POAG) being the most common form. (Braunger et al., 2015; Caprioli, 2013; Quigley, 2011; Tham et al., 2014). The trabecular meshwork (TM), which maintains IOP homeostasis by generating resistance to aqueous humor outflow, is a crucial part of this mechanism (Braunger et al., 2015; Gasiorowski and Russell, 2009; Stothert et al., 2016; Xie et al., 2019). The TM is a complex, filter-like structure of connective tissue consisting of beams and sheets of extracellular matrix surrounded by TM cells that resides in the iridocorneal angle of the eye (Stamer and Clark, 2017). After aqueous humor is produced in the ciliary body, it travels through the pupil, into the anterior chamber, and exits into the Schlemm's canal through the TM (Carreon et al., 2017; Roy Chowdhury et al., 2015). When the TM fails to maintain adequate outflow,

*Corresponding author: Jie J. Zheng, Stein Eye Institute, Department of Ophthalmology, David Geffen School of Medicine at UCLA, 100 Stein Plaza, Los Angeles, CA 90095. jzheng@jsei.ucla.edu.

POAG can develop: increased outflow resistance in the TM drives increased IOP, which can damage the optic nerve and lead to vision loss (Caprioli, 2013; Kwon et al., 2009).

Glucocorticoids, such as Dexamethasone (Dex), are used clinically to decrease inflammation, but use in the eye can increase outflow resistance in the TM and therefore elevate IOP (Fini et al., 2017). Because similar changes occur in POAG TM, glucocorticoid-treated TM cells are viewed as an *in vitro* model system (Gasiorowski and Russell, 2009; Tamm, 2002; Wordinger and Clark, 1999). A hallmark of Dex-treated TM cells is the upregulation of myocilin, a protein also linked to glaucoma pathogenesis (Stone et al., 1997; (Gasiorowski and Russell, 2009; Kwon et al., 2009). Previous studies have shown that myocilin localizes to the mitochondria, where it may have pro-apoptotic effects including reducing membrane potential (Sakai et al., 2007; Stothert et al., 2016; Wentz-Hunter et al., 2002). Furthermore, mitochondrial damage has been observed in the TM of patients with glaucoma (Izzotti et al., 2010). Given this association between POAG pathogenesis and TM mitochondria, we decided to characterize the metabolic profile of Dex-treated primary human TM cells. We employed extracellular flux (XF) analysis to quantify metabolic activity at the cellular level by measuring the oxygen consumption rate (OCR) and the extracellular acidification rate (ECAR).

In the study, we used four TM tissues obtained from four independent donors. The first TM (TM 223) was from a 70-year-old female donor. The second TM (TM 248A) was from a 67-year-old Caucasian female donor. The third TM (TM 301) was from a 60-year-old Caucasian male donor. The fourth TM (TM 303) was from a 68-year-old Asian male donor. TM cells were isolated from tissue using blunt dissection and plated on 6-well plates coated with 0.5% filtered gelatin in water. The TM cells were cultured in Dulbecco's Modified Eagle's Medium (DMEM) with GlutaMAX containing 1g/L-D-glucose, 110 mg/L Sodium Pyruvate, 10% Fetal Bovine Serum (FBS), and 1% 100x Antibiotic-Antimycotic or Penicillin-Streptomycin (Keller et al., 2018). The medium was changed every 2-3 days. Once confluency was reached, the cells were passaged to a new plate. Medium was removed and the cells were rinsed three times with Dulbecco's phosphate-buffered saline (DPBS). Enough 0.25% trypsin with ethylenediaminetetraacetic acid (EDTA) was added to cover the wells, and the cells were incubated at 37°C and 5% CO_2 for five minutes. Medium was added to neutralize trypsin and cells were resuspended and placed in a new gelatin-coated container. Cells were allowed 24 hours to adhere, and regular culturing methods were resumed.

The four TM cells, TM 223, TM 248A, TM 301 and TM 303, had spindle-like, fibroblastic morphology (Fig. 1A–D), matching previous descriptions (Keller et al., 2018; Stamer and Clark, 2017). As Dex-induced myocilin expression is the principal marker for TM cells (Gasiorowski and Russell, 2009), we used qPCR to conduct further validation. Treatments of the TM cells with Dex were started after the cells reached confluence. Half of the wells were treated with 100nM Dex dissolved in dimethyl sulfoxide (DMSO) and the other half acted as the vehicle control. Medium with Dex or vehicle was changed daily for five days. Following five-day Dex treatment, total cellular RNA was extracted from TM cells using the Qiagen RNeasy mini kit (Qiagen, Valencia, CA) as per manufacturer's protocol. The concentration of RNA was analyzed using a NanoDrop 2000 (ThermoFisher, Waltham,

MA) and the quality of the RNA was determined on the ratio of absorbance at 260 nm and 280 nm. Quantitative PCR was accomplished using qScript-XLT 1-Step RT-qPCR kit from Quanta Biosciences (Beverly, MA) per manufacturer's instructions on a Realplex 2 (Eppendorf, Hauppauge, NY) with TaqMan primers for human *GAPDH* (Hs02758991_g1) and human *MYOC* (Hs00165345_m1) purchased from ThermoFisher Scientific (Canoga Park. CA). *GAPDH*-normalized *MYOC* fold changes of each TMs were determined by the Delta-Delta Ct method. We found that Dex increased *MYOC* expression by 10.1 ± 0.1 fold (TM 223), 19.8 ± 0.1 fold (TM 248A), 17.2 ± 0.4 fold (TM 301), and 19.0 ± 0.6 fold (TM 303) (data not shown), confirming that all four cells are TM cells.

For the extracellular flux analysis, we utilized the Seahorse XF96 Flux Analyzer and performed the Mito Stress Test (Zhang and Zhang, 2019), which took 70-104 minutes. The Mito Stress Test includes sequential injection of the ATP Synthase inhibitor oligomycin, the chemical uncoupler carbonyl cyanide-p-trifluoromethoxyphenylhydrazone (FCCP), and the Complex I and III inhibitors rotenone and antimycin A. Six main parameters are determined by oxygen consumption rate (OCR) analysis: basal respiration, ATP-linked respiration, proton leak, maximal respiration, spare respiratory capacity (SRC), and non-mitochondrial respiration. Basal respiration provides information on respiration driven by ATP synthesis (ATP demand) and proton leak in the cell. The addition of oligomycin will decrease respiration that is coupled to ATP synthesis (ATP-linked respiration). The remaining respiration is due to proton leak (dissipation of the gradient through other means than ATPase) and can be used to calculate ATP-linked respiration (basal OCR – proton leak). FCCP, a protonophore uncoupler, is then added to induce maximal respiration by dissipating the proton gradient created by the ETC. Maximal respiration is calculated as the highest OCR after injection of FCCP. Lastly, antimycin-A, a complex III inhibitor, and rotenone, a complex I inhibitor, halt ETC activity altogether, thereby halting all mitochondrial oxygen consumption. The remaining OCR level represents the non-mitochondrial oxygen consumption, which is subtracted from the other measurements before analysis. Finally, the difference between maximal and basal respiration represents the spare respiratory capacity, also called reserve capacity, which can indicate a cell's ability to respond to increased energy demands. This is demonstrated schematically in Figure 1I. ATP production rate can be defined as mitochondrial (produced through oxidative phosphorylation, or OxPhos) or glycolytic, produced through glycolysis. ATP production rate was calculated as described by Divakaruni et al. (Divakaruni et al., 2017). ECAR is simultaneously measured (traces not shown) and can be used to calculate basal ECAR, ECAR levels before compound addition, and glycolytic reserve, which is similar to spare respiratory capacity, but for glycolysis. Glycolytic reserve indicates ability to increase glycolytic activity in response to demand or the closeness of a cell's glycolytic flux to its maximum (Divakaruni et al., 2014).

Two central cellular processes to produce energy as ATP are aerobic respiration and anaerobic glycolysis (Green et al., 2014). In aerobic respiration, which occurs in the mitochondria, the majority of ATP is made through oxidative phosphorylation (OxPhos) that consumes oxygen in the process. The change in extracellular oxygen concentration is measured as the OCR (oxygen consumption rate), which we use as a proxy for mitochondrial respiratory activity (Zhang and Zhang, 2019). ATP can also be made through anaerobic glycolysis, a process which ultimately produces protons ($lactate^- + H^+$).

These protons acidify the surrounding media and are measured as ECAR (extracellular acidification rate), a proxy for glycolytic activity. Oxygen is not consumed by anerobic glycolysis. Thus, by utilizing XF analysis of OCR and ECAR in this study, we quantify the effect of Dex-treatment on the metabolism of TM cells.

For the XF measurement, each cell strain was at passage three. TM cells were plated and treated on a Seahorse XF analyzer 96-well microplate. Cells were not plated on the outer ring of the 96-well plate to avoid edge effects. Four experiments were performed on different days, one for each sample tissue, with each culture plated in 4-5 technical replicates. The assay was prepared according to established procedure (Divakaruni et al., 2014). On the day of the assay, the cells were washed twice to replace growth medium with DMEM assay medium consisting of 10mM glucose, 2mM glutamine, 1mM pyruvate, and 5 mM HEPES. A cartridge with O_2 and pH fluorophore sensors was hydrated overnight and calibrated before the cell plate was inserted into the Seahorse XF96 Flux Analyzer. The cells were washed twice with assay medium, removing the Dex and incubated for 30 minutes before starting the assay. During each measurement, the cartridge created a 2.28μL transient microchamber where changes in oxygen concentration and pH were measured in real time. OCR and the extracellular acidification rate (ECAR) were measured during injections of four compounds: 2.0μM oligomycin, 0.75μM FCCP injected in Ports B and C (final concentration of 0.75 μM and 1.35 μM FCCP respectively), and 2.0μM Antimycin-A and 2.0μM rotenone, which were added simultaneously. FCCP was injected twice to ensure that maximal respiration was achieved during the assay. Oxygen consumption was normalized to cell number per well after the assay and OCR is reported in pmol O_2 per minute per 10^3 cells. Cell number per well was quantified by staining the cells with Hoechst in the XF96 microplate and counting nuclei with an Operetta High Content Imaging System (PerkinElmer). Raw OCR traces for each sample are shown in Fig. 1E–H.

Results from the Mito Stress Test demonstrate that while basal respiration was not consistently affected (n=4, ns) (Fig. 2A), Dex-treated cells had maximal respiration values 1.36 ±0.082 times higher than vehicle cells (n=4, $P<0.001$) (Fig. 2B) and SRC values 1.41 ±0.18 times larger than vehicle cells (n=4, $P<0.001$) (Fig. 2C). ATP-linked respiration was 1.50 ±0.36 times higher in Dex-treated cells than in vehicle cells (Fig. 12E). Non-mitochondrial oxygen consumption was also 1.73 ±0.38 times larger than vehicle cells (n=4, $P<0.05$) (Fig. 2F). ATP production rates from OxPhos increased in Dex-treated cells by 1.48 ±0.34 fold (n=4, $P<0.05$) (Fig. 2D), and the proportion of ATP production from OxPhos out of total ATP production rate was higher in Dex-treated cells, by 1.31 ±0.14 fold (n=4, $P<0.05$) (Fig. 2K). In vehicle cells, ATP production rate from OxPhos made up an average 24.5% of total ATP production rate, compared to 32.4% in Dex-treated cells (n=4, ns) (Fig. 2J). ATP production rate from glycolysis represented 75.5% of total ATP production rate in vehicle cells, versus 67.6% in Dex-treated cells (n=4, ns) (Fig. 2J). Analysis of ECAR reveals that Dex did not have a significant effect on trends of other glycolytic properties, such as glycolytic reserve, basal ECAR, and ATP production rate from glycolysis (n=4) (Fig. 2G–I). Significance was determined with a standard two-tailed T-test using fold change data. Each data point summarizes 4-5 technical replicates of a single experiment. Error bars in Fig. 2A–I reflect the standard deviation of those technical replicates. Error bars in Fig. 2J–K reflect the standard deviation of the means of each sample's technical replicates.

As showed in Fig. 1F, TM 303 cells lacked a response to oligomycin. Since TM 303 cells were otherwise consistent with the other TM cells we studied, such lacking oligomycin response is likely due to a technical error, not a biological nonresponse. Nevertheless, this affects parameters requiring oligomycin to calculate, such as ATP-linked respiration, ATP production rate from OxPhos, and glycolytic reserve, for which TM 303 cells values changed very little (Fig. 2D, 2E and 2J, 2I, respectively). When data from TM 303 cells were omitted from the analysis, ATP-linked respiration increased by 1.65 ±0.26 fold in Dex-treated cells (n=3, $P<0.05$), and ATP production rate from OxPhos increased by 1.61 ±0.28 fold in Dex-treated cells (n=3, $P<0.05$). ATP production rate from OxPhos made up an average of 29.0% of the total ATP production rate, compared to 38.7% in Dex-treated cells (n=3, ns). ATP production rate from glycolysis represented 71.0% of the total ATP production rate in vehicle-treated cells versus 61.3% in Dex-treated cells (n=3, ns).

In our study, we observed consistent results in primary TM cells from independent donors that Dex-treated cells had increased maximal respiration, SRC, ATP-linked respiration, and non-mitochondrial respiration (Fig. 2B, C, E, F, respectively), while basal respiration was not significantly affected (Fig. 2A). Furthermore, Dex increased ATP production rates from OxPhos (Fig. 2D) and increased the proportion of total ATP production coming from OxPhos (Fig. 2K).

The Dex-treated cells had a measurable increase in the proportion of total ATP production that came from OxPhos: when the data of TM 303 cell is omitted, 29% of total ATP production came from OxPhos in vehicle-treated cells versus an average of 39% in Dex-treated cells (Fig. 2J). With the data of TM 303, 24.5% of total ATP production came from OxPhos in vehicle-treated cells, compared to 32.4% in Dex-treated cells (Fig. 2J). Although these numbers are not statistically significant due to limited number of cell strains used in the study, the trend is significant: in each cell strain, Dex increased the proportion of total ATP production rate from to OxPhos by an average 31% (n=4, $p<0.05$) (Fig. 2J). Previously, it was estimated that in TM tissue, approximately three quarters of ATP production come from glycolysis and one quarter from respiration (Epstein and Anderson, 1981), and this aligns well with our data that 24.5% of ATP production in vehicle cells was produced by OxPhos (Fig. 2J). Thus, the increase in Dex-treated cells from the standard average 24.5% to 32.4% is a departure from the TM cells' normal metabolic state. Nonetheless, glycolysis remained the dominant source of ATP production in both cases, with 75.5% of ATP production from glycolysis in vehicle cells and 67.6 in Dex-treated cells (Fig. 2J), and the difference was not statistically significant. Given that TM cells reside in a largely low-oxygen environment within the eye (Beebe et al., 2014), it is not surprising that overall TM cells may rely more so on glycolysis for energy. Still, while the majority of energy utilized by TM cells appears to come from glycolysis, our data suggests Dex-treated cells depend more than untreated cells on OxPhos, also exemplified by the statistically significant increase in ATP-linked respiration (Fig. 2E). The lack of a significant and consistent effect on glycolytic properties (Fig. 2G–I) suggests Dex may not directly affect the glycolytic pathway.

Both Dex-treated TM cells express higher levels of extracellular matrix proteins, including fibronectin, collagen, and laminin (Stamer and Clark, 2017) and therefore may require

additional energy to drive this increase in transcription and translation. Increased respiratory capacity and ATP-linked respiration, as observed here, may occur to accommodate these needs. Additionally, it is known that oxidative phosphorylation produces more ATP per glucose molecule than glycolysis, up to 32 versus net 2 ATP, so an increase in energy demand to support extracellular matrix protein production may also explain Dex-treated cells' increased dependence on OxPhos for ATP production. Of note, when TM-1 cells, an immortalized TM cell line that does not upregulate myocilin upon glucocorticoid treatment (Filla et al., 2011), were treated with Dex, none of the tested parameters were significantly affected in two separate experiments (data not shown). This data further supports upregulation of myocilin as an influential factor since TM-1 cells lost some biological properties of TM cells (Gasiorowski and Russell, 2009; Keller et al., 2018).

The increase in ATP-production from OxPhos may also be connected to increased mitochondrial content and number in Dex-treated TM cells. Animal studies have found that Dex-treated mouse and bovine TM cells have more mitochondria per cell, as well as more organelles involved in protein synthesis such as endoplasmic reticula and ribosomes (Sibayan et al., 1998; Zeng et al., 2020). POAG human TM cells have significantly higher ratios of mtDNA to nuclear DNA (nDNA), indicating more mitochondria per cell (Izzotti et al., 2010). Additionally, Dex-treated mouse TM cells have larger mitochondria (Zeng 2019) and therefore potentially larger cristae, which may translate to more space for OxPhos to occur (Javadov 2018). These morphological changes could also be the cause of the observed Dex-induced increases in maximal respiration and SRC.

The Dex-induced increases in ATP production rate observed in this study may elevate levels of reactive oxygen species (ROS) in the TM. Mitochondria are one of the largest sources of ROS, and ROS are produced in the mitochondria mainly during OxPhos through the oxidation of nicotinamide adenine dinucleotide (NADH) (Izzotti et al., 2010; Sacca et al., 2015). This is consistent with our observation that the Dex-treated TM cells had larger non-mitochondrial oxygen consumption rates (Fig. 2F) which indicates higher levels of ROS production (Wang et al., 2018). Indeed, glaucomatous and Dex-treated TM cells are known to possess higher ROS levels (He et al., 2008; Izzotti et al., 2010; Sacca et al., 2015).

ROS have been recognized to play an important role in the development of glaucoma (Izzotti et al., 2010; Sacca et al., 2005). Both ROS production and damage of ROS to TM cells are linked to mitochondrial activity (He et al., 2008). Long-term ROS exposure contributes to apoptosis and mitochondrial damage (Izzotti et al., 2010), as well as decreased aqueous humor outflow at the TM (Gasiorowski and Russell, 2009) and ultimately ocular hypertension and glaucoma pathogenesis (Sacca et al., 2005). In the current study, we did not observe in the extracellular flux analysis symptoms of mitochondrial damage that may be expected from ROS in the Dex-treated TM cells. It is likely that the five-day Dex treatment may be not long enough to cause mitochondrial damage. Nonetheless, sustained increased demand on the mitochondria, as was observed in this study, especially in the low oxygen environment of the TM, may ultimately result in mitochondrial dysfunction and thus contribute to increased outflow resistance seen in Dex-treated TM. Indeed, the TM cells of POAG patients possess traits indicative of mitochondrial dysfunction, including higher levels of endogenous ROS, decreased membrane potentials, and increased sensitivity to

complex I inhibition and other secondary stressors (He et al., 2008). In addition, mtDNA is particularly susceptible to oxidative stress, and, accordingly, increased incidence of the mtDNA^{4977} deletion is a form of mitochondrial damage found in POAG patients (Izzotti et al., 2010; Yusoff et al., 2019). Mitochondrial dysfunction such as these in turn lead to a further increase in ROS levels (Sacca et al., 2015) and further cell death, thus perpetuating a cycle of damage. Given the havoc ROS can wreak on TM cells, the metabolic changes induced by Dex treatment may therefore be one causative factor for the development of glaucoma-like symptoms in Dex-treated TM, including mitochondrial damage and cell death.

Acknowledgements

We thank Dr. Donna Peters for providing TM-1 cells. This study was supported in part by NIH grants R01EY028557 and by Research to Prevent Blindness.

REFERENCES

Beebe DC, Shui YB, Siegfried CJ, Holekamp NM, Bai F, 2014. Preserve the (intraocular) environment: the importance of maintaining normal oxygen gradients in the eye. Jpn J Ophthalmol 58, 225–231. [PubMed: 24687817]

Braunger BM, Fuchshofer R, Tamm ER, 2015. The aqueous humor outflow pathways in glaucoma: A unifying concept of disease mechanisms and causative treatment. Eur J Pharm Biopharm 95, 173–181. [PubMed: 25957840]

Caprioli J, 2013. Glaucoma: a disease of early cellular senescence. Invest Ophthalmol Vis Sci 54, ORSF60–67. [PubMed: 24335071]

Carreon T, van der Merwe E, Fellman RL, Johnstone M, Bhattacharya SK, 2017. Aqueous outflow - A continuum from trabecular meshwork to episcleral veins. Prog Retin Eye Res 57, 108–133. [PubMed: 28028002]

Divakaruni AS, Paradyse A, Ferrick DA, Murphy AN, Jastroch M, 2014. Analysis and interpretation of microplate-based oxygen consumption and pH data. Methods Enzymol 547, 309–354. [PubMed: 25416364]

Divakaruni AS, Wallace M, Buren C, Martyniuk K, Andreyev AY, Li E, Fields JA, Cordes T, Reynolds IJ, Bloodgood BL, Raymond LA, Metallo CM, Murphy AN, 2017. Inhibition of the mitochondrial pyruvate carrier protects from excitotoxic neuronal death. J Cell Biol 216, 1091–1105. [PubMed: 28254829]

Epstein DL, Anderson PJ, 1981. In vitro biochemistry of trabecular meshwork. Vision Res 21, 161. [PubMed: 7269288]

Filla MS, Schwinn MK, Nosie AK, Clark RW, Peters DM, 2011. Dexamethasone-associated cross-linked actin network formation in human trabecular meshwork cells involves beta3 integrin signaling. Invest Ophthalmol Vis Sci 52, 2952–2959. [PubMed: 21273548]

Fini ME, Schwartz SG, Gao X, Jeong S, Patel N, Itakura T, Price MO, Price FW Jr., Varma R, Stamer WD, 2017. Steroid-induced ocular hypertension/glaucoma: Focus on pharmacogenomics and implications for precision medicine. Prog Retin Eye Res 56, 58–83. [PubMed: 27666015]

Gasiorowski JZ, Russell P, 2009. Biological properties of trabecular meshwork cells. Exp Eye Res 88, 671–675. [PubMed: 18789927]

Green DR, Galluzzi L, Kroemer G, 2014. Cell biology. Metabolic control of cell death. Science 345, 1250256. [PubMed: 25237106]

He Y, Leung KW, Zhang YH, Duan S, Zhong XF, Jiang RZ, Peng Z, Tombran-Tink J, Ge J, 2008. Mitochondrial complex I defect induces ROS release and degeneration in trabecular meshwork cells of POAG patients: protection by antioxidants. Invest Ophthalmol Vis Sci 49, 1447–1458. [PubMed: 18385062]

Izzotti A, Sacca SC, Longobardi M, Cartiglia C, 2010. Mitochondrial damage in the trabecular meshwork of patients with glaucoma. Arch Ophthalmol 128, 724–730. [PubMed: 20547950]

Keller KE, Bhattacharya SK, Borras T, Brunner TM, Chansangpetch S, Clark AF, Dismuke WM, Du Y, Elliott MH, Ethier CR, Faralli JA, Freddo TF, Fuchshofer R, Giovingo M, Gong H, Gonzalez P, Huang A, Johnstone MA, Kaufman PL, Kelley MJ, Knepper PA, Kopczynski CC, Kuchtey JG, Kuchtey RW, Kuehn MH, Lieberman RL, Lin SC, Liton P, Liu Y, Lutjen-Drecoll E, Mao W, Masis-Solano M, McDonnell F, McDowell CM, Overby DR, Pattabiraman PP, Raghunathan VK, Rao PV, Rhee DJ, Chowdhury UR, Russell P, Samples JR, Schwartz D, Stubbs EB, Tamm ER, Tan JC, Toris CB, Torrejon KY, Vranka JA, Wirtz MK, Yorio T, Zhang J, Zode GS, Fautsch MP, Peters DM, Acott TS, Stamer WD, 2018. Consensus recommendations for trabecular meshwork cell isolation, characterization and culture. Exp Eye Res 171, 164–173. [PubMed: 29526795]

Kwon YH, Fingert JH, Kuehn MH, Alward WL, 2009. Primary open-angle glaucoma. N Engl J Med 360, 1113–1124. [PubMed: 19279343]

Quigley HA, 2011. Glaucoma. Lancet 377, 1367–1377. [PubMed: 21453963]

Roy Chowdhury U, Hann CR, Stamer WD, Fautsch MP, 2015. Aqueous humor outflow: dynamics and disease. Invest Ophthalmol Vis Sci 56, 2993–3003. [PubMed: 26024085]

Sacca SC, Pascotto A, Camicione P, Capris P, Izzotti A, 2005. Oxidative DNA damage in the human trabecular meshwork: clinical correlation in patients with primary open-angle glaucoma. Arch Ophthalmol 123, 458–463. [PubMed: 15824217]

Sacca SC, Pulliero A, Izzotti A, 2015. The dysfunction of the trabecular meshwork during glaucoma course. J Cell Physiol 230, 510–525. [PubMed: 25216121]

Sakai H, Shen X, Koga T, Park BC, Noskina Y, Tibudan M, Yue BY, 2007. Mitochondrial association of myocilin, product of a glaucoma gene, in human trabecular meshwork cells. J Cell Physiol 213, 775–784. [PubMed: 17516541]

Sibayan SA, Latina MA, Sherwood ME, Flotte TJ, White K, 1998. Apoptosis and morphologic changes in drug-treated trabecular meshwork cells in vitro. Exp Eye Res 66, 521–529. [PubMed: 9628799]

Stamer WD, Clark AF, 2017. The many faces of the trabecular meshwork cell. Exp Eye Res 158, 112–123. [PubMed: 27443500]

Stothert AR, Fontaine SN, Sabbagh JJ, Dickey CA, 2016. Targeting the ER-autophagy system in the trabecular meshwork to treat glaucoma. Exp Eye Res 144, 38–45. [PubMed: 26302411]

Tamm ER, 2002. Myocilin and glaucoma: facts and ideas. Prog Retin Eye Res 21, 395–428. [PubMed: 12150989]

Tham YC, Li X, Wong TY, Quigley HA, Aung T, Cheng CY, 2014. Global prevalence of glaucoma and projections of glaucoma burden through 2040: a systematic review and meta-analysis. Ophthalmology 121, 2081–2090. [PubMed: 24974815]

Wang S, Shi X, Wei S, Ma D, Oyinlade O, Lv SQ, Ying M, Zhang YA, Claypool SM, Watkins P, Xia S, 2018. Kruppel-like factor 4 (KLF4) induces mitochondrial fusion and increases spare respiratory capacity of human glioblastoma cells. J Biol Chem 293, 6544–6555. [PubMed: 29507094]

Wentz-Hunter K, Ueda J, Shimizu N, Yue BY, 2002. Myocilin is associated with mitochondria in human trabecular meshwork cells. J Cell Physiol 190, 46–53. [PubMed: 11807810]

Wordinger RJ, Clark AF, 1999. Effects of glucocorticoids on the trabecular meshwork: towards a better understanding of glaucoma. Prog Retin Eye Res 18, 629–667. [PubMed: 10438153]

Xie X, Akiyama G, Bogarin T, Saraswathy S, Huang AS, 2019. Visual Assessment of Aqueous Humor Outflow. Asia Pac J Ophthalmol (Phila).

Yusoff AAM, Abdullah WSW, Khair S, Radzak SMA, 2019. A comprehensive overview of mitochondrial DNA 4977-bp deletion in cancer studies. Oncol Rev 13, 409. [PubMed: 31044027]

Zeng W, Wang W, Wu S, Zhu X, Zheng T, Chen X, Ren J, Gong Y, Ke M, 2020. Mitochondria and Autophagy Dysfunction in Glucocorticoid-Induced Ocular Hypertension/Glaucoma Mice Model. Curr Eye Res 45, 190–198. [PubMed: 31425668]

Zhang J, Zhang Q, 2019. Using Seahorse Machine to Measure OCR and ECAR in Cancer Cells. Methods Mol Biol 1928, 353–363. [PubMed: 30725464]

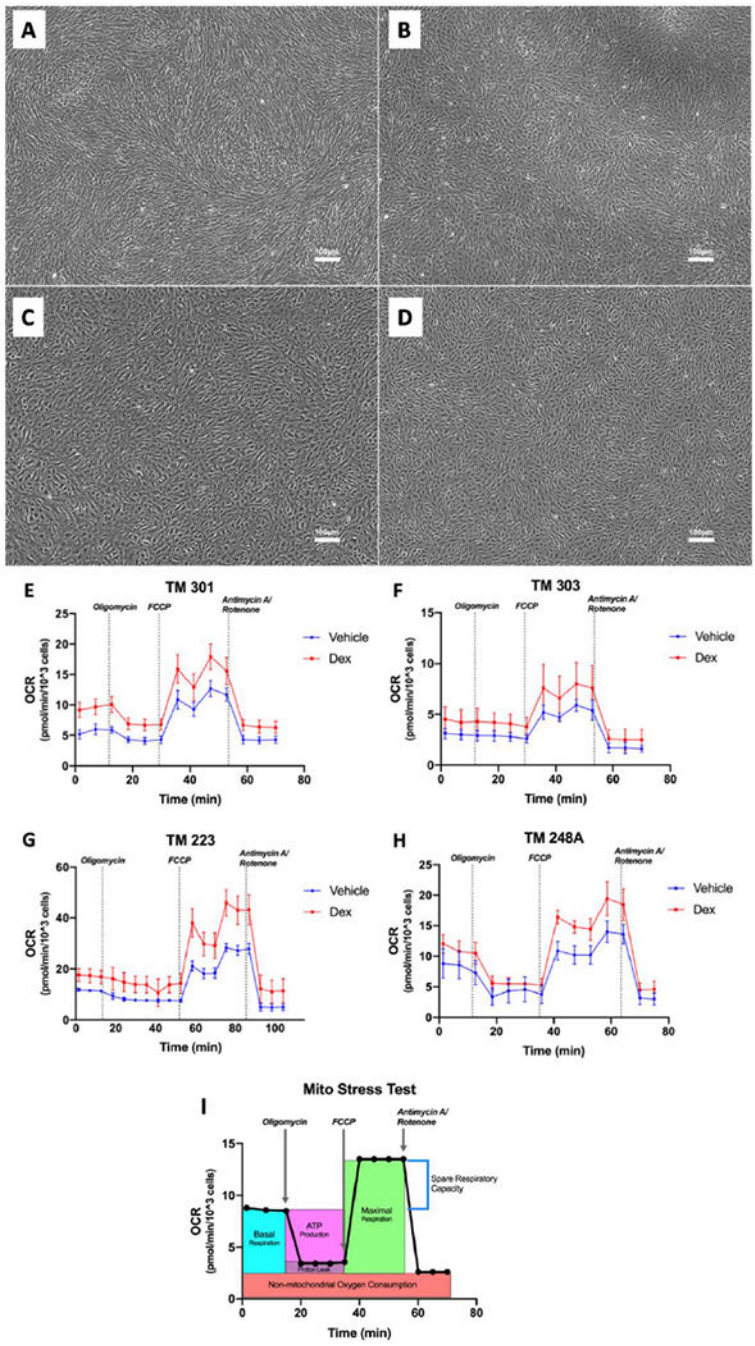

Fig. 1.

Cell imaging of four human TM samples used in the study (A-D) and the oxygen consumption rates (OCRs) of the four cells during the Seahorse extracellular flux (XF) measurement (E-H). Schematic diagram of typical XF trace, demonstrating how each parameter is determined (I).

(A) TM 303 cells at passage 1; (B) TM 301 cells at passage 1; TM 223 cells at passage 1 (C); and TM 248A cells at passage 1 (D). Before being analyzed with the XF Cell Mito Stress Test assay, the cells were treated with 100nM Dex or vehicle DSMO for five days.

The OCRs of the four cells (E-H) were measured throughout injections of four compounds (2.0μM oligomycin, 0.75μM FCCP, 2.0μM Antimycin-A and 2.0μM rotenone), and the dotted lines indicate injection times. (E) TM 301 cells; (F) TM 303 cells; (G) TM 223 cells; and (H) TM 248A cells. Each data point of E-H summarizes 4-5 technical replicates of a single experiment. Error bars reflect standard deviation of those technical replicates.

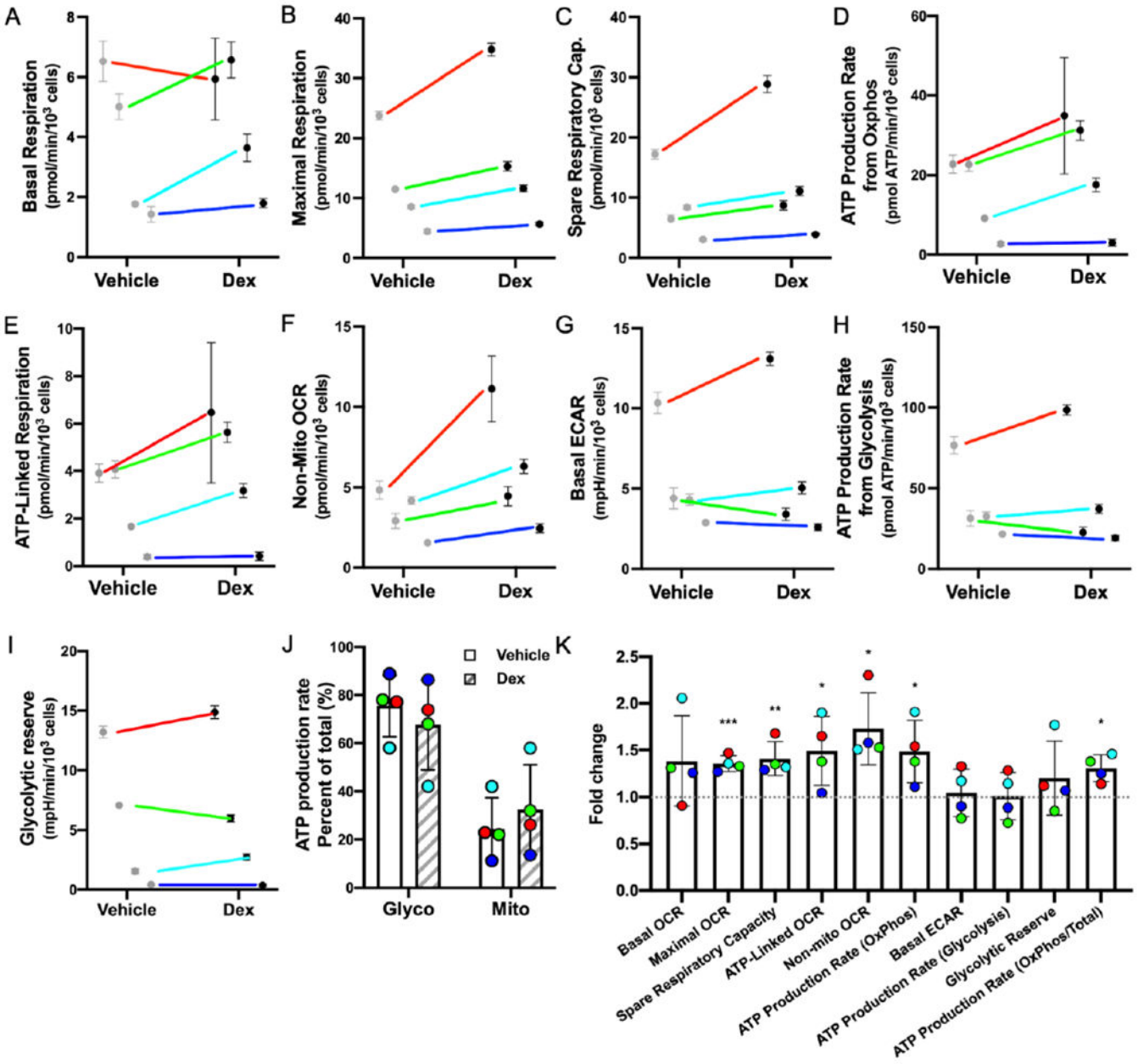

Fig. 2.

Data calculated from the XF analysis. A-J reflect the raw OCR and ECAR data for each parameter and sample. K is a summary diagram demonstrating the fold change and significance values for each parameter.

Dex did not significantly or consistently affect basal respiration (n=4, ns) (A), but Dex-treated cells had increased maximal respiration (n=4, P<0.001) (B), spare respiratory capacity (n=4, P<0.01) (C), ATP production rate from OxPhos (n=4, P<0.05) (D), ATP-linked respiration (n=4, P<0.05) (E), and non-mitochondrial oxygen consumption (n=4, P<0.05) (F) compared to vehicle cells. Glycolytic properties, basal ECAR (n=4, ns) (G), ATP production rate from glycolysis (n=4, ns) (H), and glycolytic reserve (n=4, ns) (I),

were not significantly or consistently affected. The share of total ATP production from OxPhos was increased in Dex cells while the share of ATP production from glycolysis was decreased (n=4, ns) (J). These changes were consistent between each strain but not statistically significant. K summarizes the fold change significance data for parameters A-I as well as the proportion of ATP production rate from OxPhos out of total, which was increased in Dex-treated cells (n=4, $P<0.05$) (K). Each data point is the average fold change of Dex-treated cells compared to vehicle cells which were normalized to one, as represented by the dotted line. TM223 is colored red, TM248A is green, TM 301 is light blue, and TM 303 is dark blue.

(*) indicates $p < 0.05$. (**) indicates $p < 0.01$. (***) indicates $p < 0.001$. Each data point summarizes 4-5 technical replicates of a single experiment. Error bars in A-I reflect standard deviation of those technical replicates. Error bars in J-K reflect standard deviation of the means of each sample's technical replicates. Significance was determined with a standard two-tailed T test using fold change data.